Laser Ultrasonic Inspection of Environmental Barrier Coatings

T. W. Murray[†] and O. Balogun

Abstract The mechanical properties of mullite ($3Al_2O_3\ 2SiO_2$) environmental barrier coatings are determined using a laser-based ultrasonic system. The waveforms generated by a laser source in mullite coatings in the 1-20 μm thickness range are evaluated theoretically using the integral transform technique. It is shown that the laser source generated the two lowest order SAW modes in these systems. Experimental waveforms are generated using a 600ps pulsed Nd:YAG microchip laser and detected using a stabilized Michelson interferometer. The dispersion curves for the generated modes are extracted from the experimental data and the mechanical properties of the coatings are obtained by minimizing the error between the measured and calculated velocity values. The waveforms generated in mullite coatings agree well with theory and laser-based ultrasonics is shown to provide an effective tool for the nondestructive evaluation of ceramic coatings.

1. Introduction

Mullite ($3Al_2O_3\ 2SiO_2$) is an important engineering ceramic exhibiting excellent high-temperature strength, low thermal expansion, and good chemical stability. Mullite is a candidate material for corrosion resistant coatings on silicon based ceramics (SiC and Si_3N_4) that are susceptible to hot-corrosion when used in hostile environments. This paper presents a theoretical and experimental analysis of laser generation of ultrasound in mullite environmental barrier coatings (EBCs) grown by CVD. A model recently developed for laser generated ultrasound in layered isotropic plates is used to study the wave modes generated in EBCs with thicknesses in the 1-20 μm range, and it is shown that multiple surface acoustic wave modes are generated in these coatings. Using the 2-D FFT technique (Alleyne and Cawley, 1991) the SAW modes, which are overlapping in the time domain, can be separated and the density, elastic modulus,

and Poisson's ratio determined.

Optical techniques for the generation and detection of ultrasound have received considerable attention and have been utilized in a wide variety of nondestructive evaluation (NDE) and materials characterization applications (Scruby and Drain, 1990; Davis et al., 1993; Hutchins, 1986; Monchalin et al., 1998). Laser ultrasonic techniques have been shown to be particularly well suited for the inspection of thin films and coatings and several techniques have been utilized including: a pump-probe technique in which very high frequency (GHz) acoustic waves are generated that propagate perpendicular to the film and reflect off the film/substrate interface (Thomsen et al., 1986)., the impulsive stimulated thermal scattering (ISTS) technique demonstrated in Duggal et al .(1992) and Rogers, (2000) and the phase velocity scanning (PVS) technique used in Cho et al. (1998) which both use a spatially periodic irradiance pattern to generate single frequency surface acoustic wave

(SAW) tone-bursts, and broadband techniques demonstrated in, for example, (Schneider et al., 1995) and (Shen and Hess, 1997) where SAW's are generated with a simple pulsed laser point or line source. The pump-probe technique requires an ultrafast laser source and attenuation limits the useful measurement range to relatively thin films making it less suitable for the inspection of EBCs which can be tens of microns thick. The broadband technique has the advantages over the ISTS and PVS techniques in that, provided sufficient signal-to-noise ratio is possible, information can be obtained about a materials system over a wide bandwidth in a single experiment. In contrast, the ISTS and PVS technique typically probe the specimen at a single discrete frequency per experiment, and thus the dispersion curve must be found point-by-point over the frequency range of interest. Note that recently a modification of the ISTS technique has been developed which allows for several narrowband signals to be generated simultaneously allowing for more rapid data collection (Rogers et al., 2000).

In this paper, the broadband technique will be used where surface acoustic waves SAWs are generated by a point focused laser and detected using an interferometer. SAWs are confined to propagate in the near surface region and are thus very sensitive to the properties of surface coatings. Unlike SAWs which propagate on a half-space, SAWs which propagate on a coating/substrate system are dispersive (Farnell and Adler, 1972). The penetration depth of SAWs depends on their wavelength allowing us to probe the elastic properties as a function of depth. High frequency (short wavelength) SAWs interact primarily with the near surface region while low frequency (long wavelength) SAWs penetrate further into the substrate. Measurement of the dispersion of SAWs over a wide frequency bandwidth makes it possible to extract the elastic properties, density, and thickness of single and multilayer films. In addition, SAWs can be used to monitor damage in coatings as the velocity and attenuation of SAWs are sensitive to the presence of microcracking, porosity, residual stress, and machining texture (Pecorari, 2000, 2001; Schneider et al., 1999).

2. Theory

Pulsed laser sources provide a nondestructive, non-contact means of wide-bandwidth acoustic wave generation. In order to determine the properties of a given structural system, the signal generated by a laser source in such a system must be well understood. The laser generation of ultrasound in a half space as well as in thin plates has previously been addressed by Spicer et al. (1990, 1991), McDonald (1990), Cheng et al. (1994), and Sanderson et al. (1997). The work of these papers was recently extended to the case of single and multi-layer films and coatings by Murray et al. (1999) and Cheng et al. (2001). The integral transform technique is used to calculate the response of a layered system to an axisymmetric laser source. The model will be briefly reviewed below for the specific case of a single isotropic coating on a semi-infinite substrate and both time domain displacements and dispersion curves presented for mullite EBCs.

The axially symmetric elastic wave problem is set up in cylindrical coordinates with the decomposition of the displacement component normal to the surface (note that this is the component measured with the interferometric detection system) is written as:

$$u_z = \varphi_{,r} - \psi_{,z} \qquad \text{.........(1)}$$

The vector potential is given by ψ (θ component only) and the scalar potential by φ. The two potentials satisfy the following wave equations:

$$\varphi_{,rr} + \frac{1}{r}\varphi_{,r} + \varphi_{,zz} = s_L^2 \varphi_{,tt} \qquad \text{.........(2)}$$

$$\psi_{,rr} + \frac{1}{r}\psi_{,r} + \psi_{,zz} - \frac{1}{r^2}\psi = s_T^2 \psi_{,tt} \qquad \text{.........(3)}$$

where $s_L = 1/c_L$ and $s_T = 1/c_T$ are the slownesses

of the longitudinal and transverse waves in the coating with the corresponding phase velocities c_L and c_T . Analogous equations follow for the substrate. These equations are augmented by the initial conditions. If the system is at rest prior to t = 0 then for both the coating and substrate:

$$\varphi(r,z,0) = \varphi_{,t}(r,z,0) = \psi(r,z,0) = \psi_{,t}(r,z,0) = 0 \quad \cdots (4)$$

The boundary conditions to be satisfied at the coating/substrate interface are given as:

$$\tau^1_{zz} = \tau^2_{zz} \quad \tau^1_{zr} = \tau^2_{zr} \quad u^1_{r} = u^2_{r} \quad u^1_{z} = u^2_{z}$$

$$\cdots\cdots (5)$$

where the superscripts (1,2) indicate the film and substrate respectively. Eqns. (2) through (5) are solved using a transform technique. A Laplace transform is applied with respect to the temporal variable and a Hankel transform with respect to the radial coordinate. The equations must be supplemented by the appropriate traction boundary conditions at the coating surface. Taking the Hankel-Laplace transform of eqns. (2) and (3) and solving the resulting expressions for the potentials yields:

$$\varphi^1_{LH0} = Ae^{-\alpha 1z} + Be^{\alpha 1z}$$
$$\psi^1_{LH1} = Ce^{-\beta 1z} + De^{\beta 1z} \qquad \cdots\cdots (6)$$

in the coating, and

$$\varphi^2_{LH0} = Ee^{-\alpha 2z}$$
$$\psi^2_{LH1} = Ge^{-\beta 2z} \qquad \cdots\cdots (7)$$

in the substrate, where:

$$\alpha^2(1,2) = {s^2}\big/{c^2_L(1,2)} + p^2 \quad and \quad \beta^2(1,2) = {s^2}\big/{c^2_T(1,2)} + p^2$$

p is the Hankel transform variable and s is the Laplace transform variable. The subscript L refers to the Laplace transform and the subscripts $H0$ and $H1$ refer to Hankel transforms of order zero and unity, respectively. The constants A-G must be determined by evaluating the boundary conditions.

The boundary conditions at the coating/substrate have already been given in eqn. 5 and leaving the boundary conditions at the top surface to be determined. It has been shown by (Spicer et al., 1990; 1991) that in a number of practical cases of interest, the thermoelastic source can be modeled as an equivalent elastic boundary source. The following Hankel-Laplace transformed boundary conditions may be used at the coating surface (z = 0):

$$\tau^{LH0}_{zz} = -\frac{(\beta^2 + p^2)}{s\varepsilon} NQ_o Q(p)Q(s)$$
$$\tau^{LH1}_{rz} = -2(\frac{p}{s})NQ_o Q(p)Q(s) \qquad \cdots\cdots (8)$$

where: , $\varepsilon^2 = \frac{s}{\kappa} + \alpha^2$ k is the thermal diffusion coefficient, and N is a constant related to the thermal and elastic properties of the top coating. $Q(p)$ and $Q(s)$ are the Hankel transform of the incident laser pulse spatial profile and the Laplace transform of the laser pulse temporal profile, respectively, and Q_0 is the absorbed laser energy. The laser source function has been given by

$$Q(r,t) = Q_0 \left[\frac{2}{R^2} e^{-\frac{2r^2}{R^2}} \right]\left[\frac{8t^3}{\tau^4} e^{-\frac{2t^2}{\tau^2}} \right] \qquad \cdots\cdots (9)$$

where R is the laser spot size and τ is the laser pulse rise time. This source has been shown to accurately represent the stress field induced by a laser in a number of practical cases (Spicer et. al., 1990, 1991; Murray et. al., 1999).

The surface boundary conditions hold under the following assumptions: the heating is localized to the film, the point of observation is outside the volume defined by significant thermal diffusion, and the optical energy is converted to heat close to the irradiated boundary. The first two assump- tions can be expected to hold, in general, if the film thickness and source-to-receiver distance are both sufficiently greater than the thermal diffusion length ($4kt$)$^{1/2}$, where t is the incident laser pulse width. The analysis is particularly suited

for the evaluation of thermal and environmental barrier coatings whose 500nm to 20 μ m thickness range is much larger than the thermal diffusion length on the imescales of interest.

Evaluation of the boundary and interface conditions yields a 6x6 matrix that is numerically inverted for the potential coefficients. Eqn. 6 is then substituted into the Hankel-Laplace transform of eq. (1) in order to find the transformed displacement solution. The displacement with respect to time and space is then obtained through numerical inversion of the transformed solution.

Figure 1 shows the dispersion curve for a mullite coating on a silicon carbide substrate. The Young's modulus, Poisson's ratio, and density of the coating and substrate are taken as E = 227.5 GPa, v = 0.28, and ρ = 3.17 g/cm^3 (Ledbetter et al., 1998) and E = 410.0 GPa, v = 0.14, and ρ = 3.10 g/cm^3, respectively. The lowest order SAW mode approaches the SAW velocity of the substrate at low frequency*thickness (fh) values (note that h refers to the thickness of the coating). This corresponds to SAWs with large penetration depths and thus the presence of the coating has little effect on the phase velocity. At higher fh values the velocity of the SAWs approaches the SAW of the coating. In this regime the penetrationdepth is small and the SAWs propagate depth is small and the SAWs propagate primarily
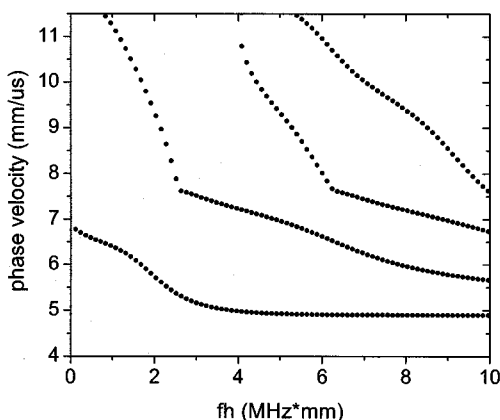
in the coating. There are several higher order SAW modes observed in the dispersion curve as well. These have a cutoff at the shear wave velocity of the substrate (7.62 mm/μ s). Above the cutoff these modes, often referred to as pseudo-Sezawa modes, radiate acoustic energy into the substrate. Below the cutoff these modes, now referred to as Sezawa modes, propagate without losing energy to the substrate and the velocity of these modes approaches the shear wave velocity of the coating at high fh values.

Figure 2 shows the time domain displacement normal to the surface in a 10 μ m thick mullite film on SiC at source-to-receiver distances ranging from 200-1000 μ m. The laser generation source spot size is 20 μ m and the rise time is 1 ns. The waveforms show that the laser source primarily generates the lowest order SAW mode. The low frequencies propagate significantly slower than the higher frequencies as expected from the dispersion curve and the waveforms exhibit a significant amount of dispersion over relatively short source-to-receiver distances. The second mode is also observed and at source to receiver distance of 800-1000 μ m the two modes are clearly separated in time with the first (low amplitude) arrival corresponding to the second mode and the latter arrival corresponding to the first mode. Figure 3 shows the normal displacement produced for in
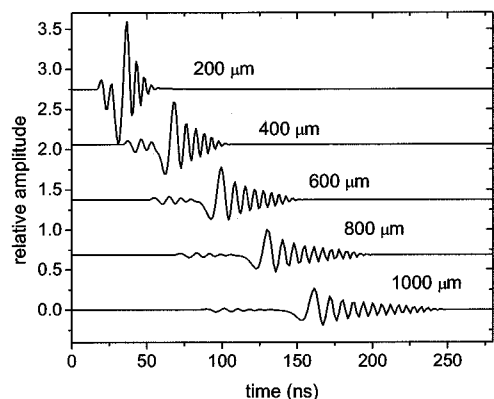

Fig. 1   Dispersion curve for a mullite coating on a SiC substrate

Fig. 2   Acoustic waves generated by a laser source in a 10 μ m thick coating on a SiC substrate at source-to-receiver distances of 200-1000 μ m

coatings with thickness ranging from 1-20 μ m and a source to receiver distance of 600 μ m. The 1 μ m thickcoating has little effect on the generated waveform which is similar to that generated on a SiC half-space with the first arrival corresponding to the surface skimming longitudinal wave and the second the SAW. This waveform shows little dispersion indicating that higher frequencies must be generated (through, for example, decreasing the generation spot size) to obtain information about the coating properties. The 5-20 μ m waveforms exhibit increasing dispersion and the two dispersive SAW modes are clearly visible.
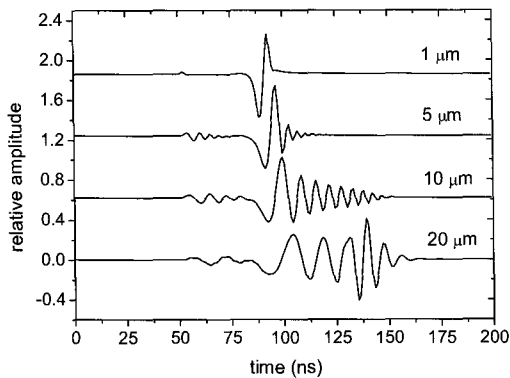

Fig. 3   Acoustic waves generated by a laser source in 1-20 μ m thick coatings with a source-to-receiver distance of 600 μ m

3. Experimental Setup

The mullite coatings were tested using the laser acoustic microscopy system illustrated in Figure 4. The system has three optical paths that lead to the sample surface through the same long working distance objective (Numerical Aperture = 0.4). The first path leads to a CCD camera and allows for optical imaging of the sample surface as well as sample alignment. In the second path, the detection laser light enters the microscope from a single mode optical fiber, is collimated, and directed to a beamsplitter where it is divided into reference and signal beams. The reference beam reflects off of a mirror mounted on an actuator (used for
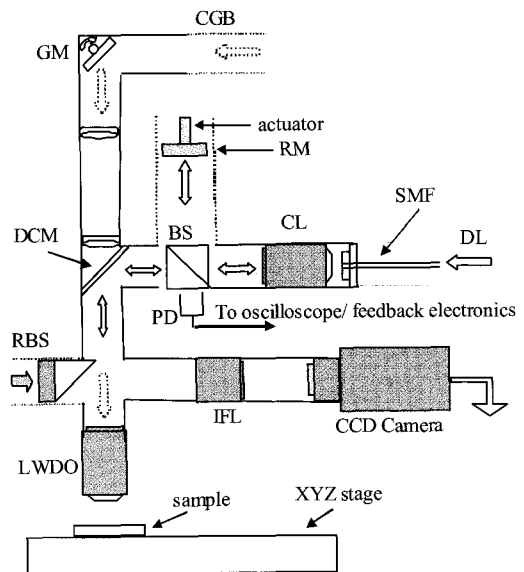

Fig. 4   Laser acoustic microscopy setup for coating inspection. Figure is labeled as follows: CGB (collimated generation beam), GM (gimbal mount), DCM (dichroic mirror), BS (beamsplitter), RM (reference mirror), SMF (single mode fiber), CL (collimating lens), DL (detection laser), PD (photodetector), RBS (removable beamsplitter), IFL (image forming lens), LWDO (long working distance objective).

stabilization) and is sent to a photodiode with a 1 GHz bandwidth. The signal beam is sent to the specimen surface and, upon reflection, returns back to the beamsplitter and interferes with the reference beam at the photodetector. The detection system thus forms a standard Michelson interferometer. Additionally, polarization optics (not shown in the figure) are used to control the amount of light sent into the reference and signal beams. The detection laser is a 200mW frequency doubled Nd:YAG (λ =532nm).

The generation laser is collimated, directed to a mirror on a gimbal mount, sent though a relay lens system, and on to the specimen. The gimbal mount allows for precise control of the generation point within the field of view (1.25 mm) of the microscope and allows the source-to-receiver distance to be controlled by adjusting the angle at

which the beam enters the objective. The source-to-receiver distance can be controlled with greater than 500nm resolution. The generation laser is a 600 ps. Nd:YAG microchip laser with a pulse energy of $10 \mu J$ which is used at the fundamental frequency (1064nm). The generation laser energy was attenuated to below $1 \mu J$ to avoid damage to the coating surface. To determine the ablation threshold, the specimen surface was observed under the optical microscope as the generation laser was increased. The ablation threshold was taken as the point where a slight discoloration of the sample surface was observed.

The laser ultrasonic system is well suited for the *local* inspection of materials properties. The source and receiver probe the sample through a single microscope objective and experiments are typically performed with a maximum source-to-receiver distance of 500-600 μ m. The use of a diffraction limited detection beam (spot size ~ 665 nm) allows us to work on specimens which are unpolished and optically rough but have localized optically flat regions where high modulation depth can be obtained using standard Michelson interferometer. The precision of our velocity measurements is limited in these experiments by the resolution of the source-to-receiver measurement (less than 500nm) and the sample rate of the digitizer (4Gs/s).

4. Results and Discussion

Figure 5 shows representative waveforms detected in a 11.2μ m mullite film at several propagation distances. The waveforms were averaged 1000 times to improve the signal-to-noise ratio. Multiple modes are observed experimentally and these modes are overlapping in time for the source to receiver distances shown. The mechanical properties of the coatings are found by first using the experimental data to determine the dispersion curves and subsequently minimizing the mean squared error between the experimental and theoretical dispersion curves using the simplex

optimization routine (Press et al., 1986). Using relatively small source to receiver distances allows for high signal-to-noise ratio measurements over a broad frequency bandwidth and minimizes the effects of high frequency signal loss due to scattering and attenuation, but at the propagation distances shown in Figure 5 the generated modes are not clearly separated in time and thus the dispersion curves can not be obtained by measuring the displacement at two distances and using the simple phase unwrapping scheme detailed in (Schneider et al., 1995).
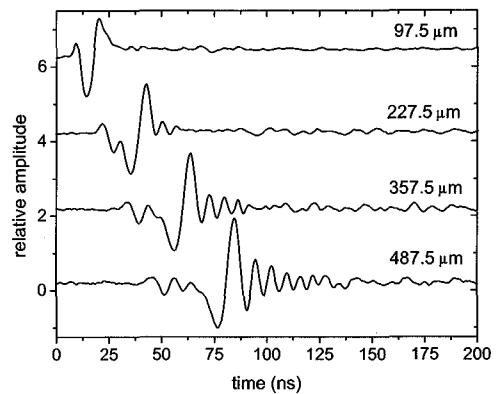

Fig. 5 Experimental waveforms measured at several source to receiver distances

The dispersion curves are found using the 2D FFT technique of (Alleyne and Cawley, 1991). A set of waveforms is collected at evenly spaced source-to-receiver intervals. One data set is illustrated in Figure 6 where 81 waveforms have been collected at intervals of every 6 μ m. At close source to receiver distances (see waveform number 1 for instance) a short arrival is observed while the latter waveforms show relatively broad arrivals in time indicating the extent of the dispersion. A 2D FFT (with respect to space and time) is then taken of the waveforms in Figure 6 resulting in the plot shown in Figure 7a. The waveforms are now in the spatial and temporal frequency domain. The peaks in the 2D FFT correspond to SAW modes and the two modes are clearly separated over a large frequency band. While the first mode has significantly higher amplitude than the second mode, the
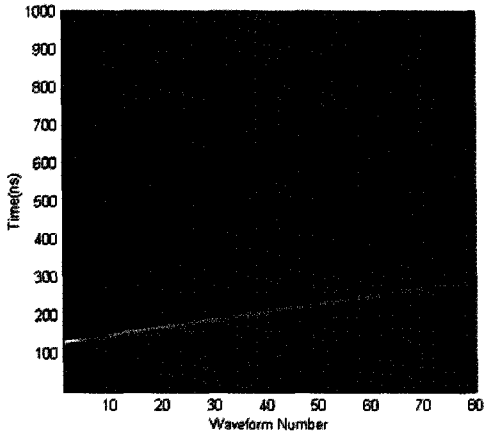
Fig. 6   Plot of 81 waveforms taken at increasing source
         to receiver distances. The propagation distance
         is increased by 6 μm increments in each trace
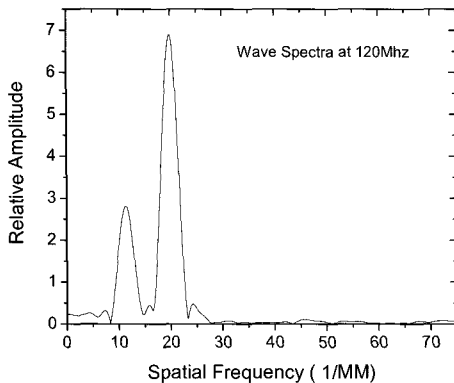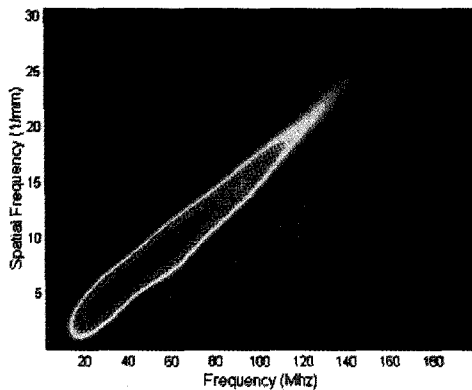

Fig. 7   a) 2D FFT of waveforms shown in Fig. 6. and
         b) a slice through the 2D FFT at 120 MHz showing
            two distinct peaks in spatial frequency
            corresponding to two modes

second mode is still clearly visible below the first mode in Figure 7a. A slice of Figure 7a at 120 MHz is shown in Figure 7b and two peaks in spatial frequency are clearly observed with the larger peak corresponding to the first mode and the smaller to the second. The dispersion curve for each of the modes was found by searching for peaks in the 2D FFT.

The dotted lines in Figure 8 shows the measured dispersion curve for the first two modes found using the this technique. The noise on the second mode is due to the small amplitude of this mode and poorer signal-to-noise ratio (SNR) with respect to the first mode. The useful frequency range of the first mode, where the highest SNR is obtained, is from 80-230 MHz. The simplex search algorithm was used to determine the mechanical properties of the coatings by minimizing the mean squared error between the measured and calculated dispersion curves. Only the first mode was used for the optimization routine due to the low SNR of the second mode. The optimization routine was used to determine the Elastic Modulus, Poisson's ratio, and density of the coating. The results from three independent experiments over separate regions of an 11.2um thick mullite coating on SiC are given in Table 1.

Table 1   Properties of 11.2 mm thick mullite coating found
          using the optimization routine.

data set	E(GPa)	ν	ρ (kg/m³)
1	188.9	.22	3022
2	190.6	.21	3043
3	188.32	.22	3086

The theoretical dispersion curves agree very well with the experimental curves and are over-plotted in Figure 8 (solid lines). The experiments from the different regions give consistent results. The values for the Elastic Modulus are somewhat lower than for fully dense mullite reported in the literature and this may be due to the presence of porosity which has a strong effect on the elastic propertie. The
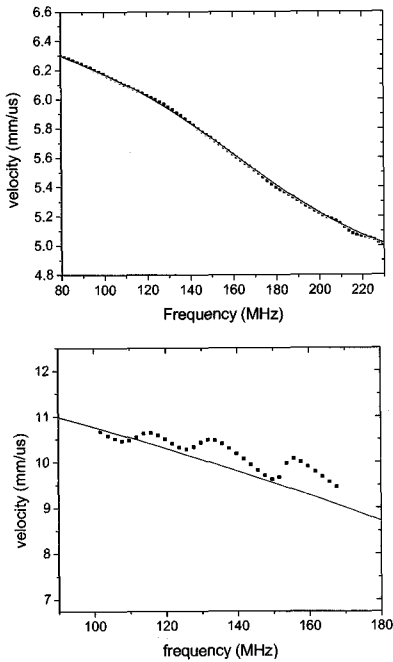
Fig. 8   Dispersion curves for a) the first mode and b) the second mode. The dotted line shows the experimental results and the solid line shows the theoretical results from the fitting routine.

density values obtained are also slightly lower than the literature values which supports this hypothesis. (Ledbetter et al., 1998) The simplex algorithm converged to the same solution with various initial guesses indicating that it had reached a global minima and that three properties can be reliably obtained for these coatings.

Figure 9 shows the time domain signals calculated using the properties found from the optimization routine. The calculated waveforms agree well with the measured waveforms for the propagation distances shown. The generation spot size was taken as 20μm for the theoretical waveforms. The frequency content of the experimental signals is slightly lower than the theoretical waveforms. This discrepancy is most likely due to high frequency grain boundary scattering in the sample which is not taken into account in the theoretical model. Nevertheless the waveforms show good agreement indicating that the model can be used for laser generated ultrasound in ceramic EBCs.
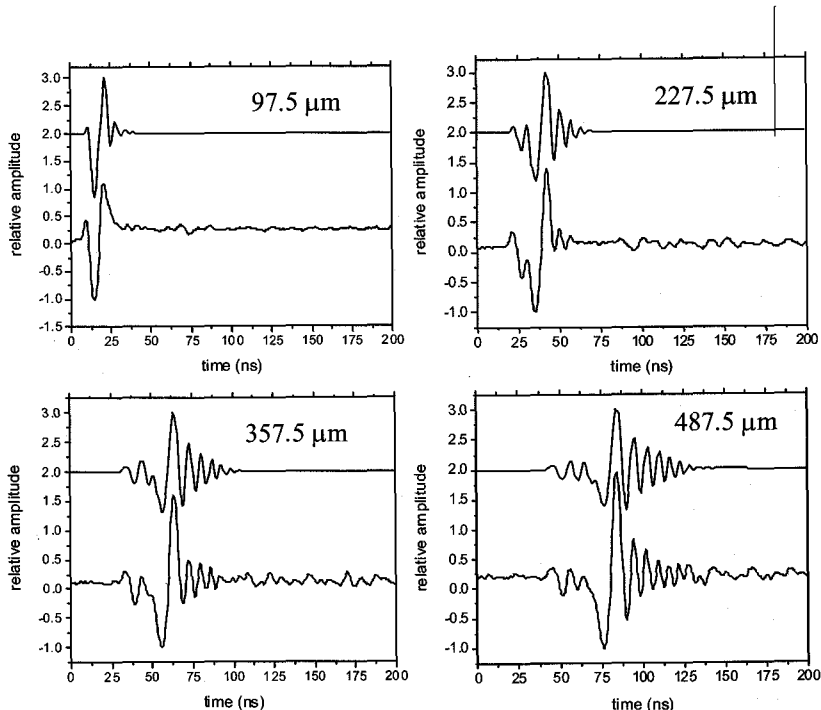

Fig. 9   Comparison of experimental and theoretical time domain waveforms in mullite. The top trace in each plot gives the theoretical waveform and the bottom the measured waveform.

5. Conclusions

A laser based ultrasonic system has been used to determine the mechanical properties of ceramic environmental coatings. The experimental waveforms show both the lowest order SAW mode as well as one higher order mode (Sezawa mode). The acoustic microscopy system presented allows for the determination of materials properties over length scales on the order of 500 μ m. The 2D FFT technique is used to separate the modes in the spatial frequency-temporal frequency domain and to map out the dispersion curves of each of the modes. The mechanical properties of the coating (density, elastic modulus, Poisson's ratio) are subsequenctly found by minimizing the mean squared error between the measured and calculated dispersion curves. The theoretical formulation for laser generated ultrasound in coatings is reviewed. The theoretical results for the mullite coatings show excellent agreement with experiment. The theoretical model can be utilized, for example, to optimize laser source parameters or as a reference in a reference based signal processing scheme to improve SNR.

Laser based ultrasonics allows for the inspection of coating materials in a completely noncontact, nondestructive manner and without prior surface preparation. This technique may also provide an effective means of monitoring coating degradation during thermal cycling. It is well known that the elastic modulus is influenced by micro-structural parameters such as micro-crack density, porosity, bonding condition within the material, and stoichiometry. Changes in the elastic modulus after thermal cycling can be monitored using laser based ultrasound. Finally, the high spatial resolution of laser-based systems can be exploited in the future to scan coating materials for crack formation prior to spallation and failure.

Acknowledgements

References

Alleyne, D., and Cawley, P. (1991) A two-dimensional Fourier transform method for the measurement of propagating multimode signals, J. Acoust. Soc. Am. 89 (3), pp. 1159

Cheng, A., Murray, T. W., and Achenbach, J. D. (2001) Simulation of laser generated ultrasonic waves in layered plates, J. Acoust. Soc. Am. 110, (2) pp. 848

Cheng, J., Wu, L., Zhang, S. (1994), Thermoelastic response of pulsed photothermal deformation of thin plates, J. Appl. Phys. 76 (2), pp. 716

Cho, H., Ogawa, S., Yamanaka, K., and Takemoto, M. (1998) Property evaluation of vapor deposited TiN film by the analysis of elastic waves, JSME Int. J. 41(3), pp. 439

Davis, S. J., Edwards, C., Taylor, G. S. and Palmer, S. B. (1993) Laser-Generated Ultrasound: its properties, mechanisms, and multifarious applications, J. Phys. D. 26(3), pp. 329-348

Duggal, A. R., Rogers, J. A. and Nelson, K. A. (1992) Real-time optical characterization of surface acoustic modes of polyimide thin-film coatings, J. Appl. Phys. 72(7), pp. 2823.

Farnell, G. W. and Adler, A. L. (1972) Elastic wave propagation in thin layers, in : Eds. Physical Acoustics, Principles and Methods, W. P. Mason Vol. 9, edited by Academic, NY

Hutchins, D. A. (1986) Mechanisms of pulsed photoacoustic generation, Can. J. Phys. 64, pp. 1247-1264

Ledbetter, H., Kim, S., Balzar, D., Crudele, S., and Kriven, W. (1998) Elastic Properties of Mullite, J. Am. Ceram. Soc. 81(4), pp. 1025-1028

McDonald, F. A. (1990) On the precursor in laser-generated ultrasound in metals, Appl. Phys. Lett. 56, pp. 230

Monchalin, J. P., Neron, C., Bussiere, J. F., Bouchard, P., Padioleau, C., Heon, R., Choquet, M., Aussel, J. D., G. Durou, and Nilson, G. (1998) Laser-ultrasonics: From the laboratory to the shop floor, Adv. Perform. Mater. 5 (1-2), pp. 7-23

Murray, T.W., Krishnaswamy, S., and Achenbach, J.D. (1999) Laser generation of ultrasound in films and coatings, Appl. Phys. Lett., 74(23), pp. 3561

Pecorari C., Lawrence, C. W., Roberts, S. G., and Briggs, G.A.D., (2000) Quantitative evaluation of surface damage in brittle materials by acoustic microscopy, Phil. Mag. A 80(11), pp. 2695

Pecorari, C. (2001) Attenuation and dispersion of rayleigh waves propagating on a cracked surface: an effective field approach, Ultrasonics 38, pp. 754-760

Press, W. H., Flannery, B. P., Teukolsky, S. A., Vetterling, W. T. (1986) Numerical Recipes, Cambridge University Press, NY

Rogers, J.A. (2000) Optical Generation and Characterization of Acoustic waves in Thin Films: Fundamentals and Applications, Annu. Rev. Mater. Sci. 30, pp. 117-157

Sanderson, T., Ume, C., and Jarzynski, J. (1997) Laser generated ultrasound: a thermoelastic analysis of the source, Ultrasonics 35, pp. 115-124

Schneider, D., Ollendorf, H., Schwartz, T. (1995) Non-destructive evaluation of the mechanical behavior of TiN-coated steels by laser induced ultrasonic waves, Appl. Phys. A 61, pp. 277-284

Schneider, D., Hammer, R., and Jurisch, M. (1999) Nondestructive testing of damage layers in GaAs wafers by surface acoustic waves, Semicond. Sci. and Technol. 14, pp. 93-98

Scruby, C. E. and Drain, L. E. (1990) Laser Ultrasonics, Techniques and Applications, Adam Hilger, N.Y.

Shen, Y. and Hess, P. (1997) Real-time detection of laser-induced transient gratings and surface acoustic wave pulses with a Michelson interferometer, J. Appl. Phys. 82(10), pp. 4758

Spicer, J. B., McKie, A. D. W., and Wagner, J.W. (1990) Quantitative theory for laser ultrasonic waves in a thin plate, Appl. Phys. Lett. 57(18), pp. 1882

Spicer, J.B. (1991) Laser Ultrasonics in Finite Structures: Comprehensive Modeling with Supporting Experiment, Ph.D. Thesis, Johns Hopkins University

Thomsen, C., Grahn, H. T., Maris, H. J., and Tauc, J. (1986) Surface generation and detec- tion of phonons by picosecond light pulses, Phys. Rev. B 34(6), pp. 4129